




# Enhanced opto-electronic properties of X-doped (X = Al, Ga, and In) CuO thin films for photodetector applications

T. Gnanasekar<sup>1,2</sup>, S. Valanarasu<sup>2,\*</sup> , Himadri Tanaya Das<sup>3</sup>, N. Chidhambaram<sup>4</sup>, R. S. Rimal Isaac<sup>5</sup>, Abdullah M. Al-Enizi<sup>6</sup>, Mohd Ubaidullah<sup>6</sup>, and Vasudeva Reddy Minnam Reddy<sup>7</sup>

<sup>1</sup> Annai Fatima College of Education, Alampatti, Thirumangalam 625706, India

<sup>2</sup> PG and Research Department of Physics, Arul Anandar College [Affiliated to Madurai Kamaraj University], Karumathur 625 514, India

<sup>3</sup> Center for Advanced Materials and Applications, Utkal University, Vanivihar, Bhubneswar, Odisha 751004, India

<sup>4</sup> Department of Physics, Rajah Serfoji Government College (Autonomous), Thanjavur, Tamil Nadu 613005, India

<sup>5</sup> Department of Nanotechnology, Noorul Islam Centre for Higher Education, Kanyakumari district, Kumarcail, Tamil Nadu 629180, India

<sup>6</sup> Department of Chemistry, College of Science, King Saud University, Riyadh 11451, Saudi Arabia

<sup>7</sup> School of Chemical Engineering, Yeungnam University, Gyeongsan 38541, Republic of Korea

Received: 13 March 2022

Accepted: 5 July 2022

Published online:

20 July 2022

© The Author(s), under exclusive licence to Springer Science+Business Media, LLC, part of Springer Nature 2022

## ABSTRACT

Recent trends in optoelectronics still need a highly efficient photodetector based on p-type metal oxide semiconductors. This work stands with the improvement in the performance of CuO thin films via doping with different metals into the thin films. The CuO thin films were successfully doped with 1 wt% of X (X = Al, Ga, and In) by spray pyrolysis method. The prepared doped CuO thin films were characterized to interpret the structural, morphological, and elemental characteristics using advanced techniques. These doped CuO thin films were subjected to study the photodetection ability by analyzing optoelectronic properties. The doping also tuned the optical and electrical properties. Among the fabricated photodetectors, the Al-doped CuO detector shows a maximum photocurrent. The CuO:Al (1.0%) thin film exhibits a high photocurrent of  $2.59 \times 10^{-6}$  A, the responsivity of  $2.82 \times 10^{-1}$  AW<sup>-1</sup>, the external quantum efficiency of 66%, and the detectivity of  $1.45 \times 10^{10}$  Jones. Compared to the other thin films, Al doping has remarkably reduced the bandgap and shows a good photosensing activity that may be due to an increase in charge carriers. These outcomes provide a way to assemble good photodetectors and tune their properties in a wide range.

Address correspondence to E-mail: valanroyal@gmail.com

## 1 Introduction

Nanomaterials are studied widely because of their great demand in the field of semiconductors. Photodetectors based on nanomaterials are at the heart of modern optoelectronic devices because they are important functional units in various energy systems and commercial applications [1–3]. Though Ge/Si-based photodetectors have been already commercialized, their high expensive manufacturing processes, unstable optoelectrical properties, high driving voltage and requirement of expensive filters for specific wavelength pay attention to low-cost, high-speed response with stable optoelectrical properties materials for photodetection purpose [4–6]. Cupric oxide (CuO), a p-type semiconductor with exclusive features has motivated researchers and industries. The abundance availability and cost-effective of CuO increases its implementation. The structural, chemical and thermal stability of CuO leads to its application in supercapacitors, batteries, biosensors, gas sensors, etc. [7, 8]. The high current conductivity, high mobility, optical absorption, and narrow bandgap of CuO prompt its utilization in photodiodes, photocatalysis, and solar cells [9–12]. Interestingly, the properties of the CuO can be governed by various parameters like synthesis methods, morphology, nanocomposites, or doping of parental nanomaterials [13–15]. The CuO thin films have been an attractive approach to developing different morphologies for optical and electrical applications. The deposition and growth of thin films can be done in various methods like dip coating, spray pyrolysis, SILAR, CVD, or electrodeposition which vary the properties of thin films [16, 17]. Zang et al. have reported nitrogen-doped CuO thin films synthesized by radical oxidation at 500 °C for reducing the resistance of thin films and enhancing optical properties [13]. The CuO thin films have been highly explored for photodetector application [17]. Quite recently, tuning of CuO thin films by dip-coating method has been reported by Das et al., for photodetector applications [16]. Similarly, the spray pyrolysis method has been reported to improve the properties of CuO thin films [18]. The spray deposition is a facile and sustainable way to develop thin films. The recently reported CuO-based heterojunction photodetector [19, 20] has demonstrated responsivity of  $0.63 \text{ AW}^{-1}$  and  $53 \text{ mA W}^{-1}$ . It is

reported that the formation of heterostructures-based photodetector results in the formation of interfacial traps and an increase in the off-current [21]. Moreover, the formation of heterostructure is a difficult process. Therefore, it is better to make a single active CuO layer for high photodetecting performance. It is known that the physical and chemical properties can be modified by controlling the amount/concentration of dopants [22, 23]. The CuO nanostructured with different dopants has been investigated for optoelectronic applications. The selected amount of La concentration is utilized while the synthesis process, to enhance the photocatalytic property of CuO without destroying its crystal structure [16]. Inass et al. have explored doping different amounts of Li (2, 4, and 6%) to the CuO thin films by the SILAR method for tuning the structural and optical nature [15]. The improved optoelectronic properties of CuO thin films after doping can be beneficial to consumer electronics. The CuO thin films also have been established with a better switching time of visible-light illumination with high photocurrent which depicts the quality of the photosensing property [24]. Furthermore, the doping effect of metals such as Li, Al, Ga, Gd, In, La, Sb, Au and Fe has been investigated highly for improving opto-electro properties [7, 9, 11, 12, 15, 22, 23, 25]. Interestingly, the doping of Ba, Sm, Au, and Pr has influenced the host structure, particle size, and optoelectronic characteristics [26–29]. The application of such doped thin films has resulted in enhanced photocurrent. Muhammad et al. have studied the experimental and theoretical effect of Al doping on CuO nanoparticles synthesized by combustion technique [30]. The DFT study has revealed the addition of impurity (Al doping) has reduced the bandgap of host CuO. The  $\text{Al}^{3+}$  has also modified the bond length and morphology of CuO nanoparticles. On other hand, indium doping to CuO thin films by the sputtering method has increased free charge concentration [31]. Single-phase monoclinic CuO:In thin films are generally used for solar cell or LED applications. Similarly, Yin et al. have studied the effect of Ni-doped CuO films with high responsivity and external quantum efficiency photodetectors [32]. All the above mentioned results evidently prove the great role of dopants in enhancing the opto-electrical properties of CuO. Among these dopants, group III elements such as Al, Ga, and In are fit for improvement of opto-electrical properties.

Joissy et al. [33] and Doni et al. [34] reported that Al can be considered the best doping element to boost the photo-current properties and they mentioned that Al element can give positive results. When Al is doped its optical properties will be modified in terms of crystalline size, optical bandgap and morphology. Further, the doped Al element significantly destabilized its highest occupied molecular orbital level and lesser its bandgap. The reduced bandgap can increase the electrical conductance implicitly resulting in a notable photo response [35]. In addition to this, the Al element will serve as an electron trapping agent and can enhance the light absorption properties [36].

Ga element can control the electrical stability of the parent element. Beside these all the three dopants ( $\text{Al}^{3+} = 0.54 \text{ \AA}$ ) ( $\text{Ga}^{3+} = 0.62 \text{ \AA}$ ) ( $\text{In}^{3+} = 0.80 \text{ \AA}$ ) has an ionic radius closer to that of  $\text{Cu}^{2+}$  ( $0.74 \text{ \AA}$ ). Therefore, it is easier for all the three dopants to replace the Cu lattice without deformation and may yield better quality and optoelectrical properties due to the minute crystal distortion. Other dopants can enlarge lattice distortions due to the major deviation in their ionic radius [31, 37, 38]. In this work, CuO and X-doped ( $X = \text{Al}$ , Ga, and In) CuO thin films were prepared on glass substrates using a simple and low-cost spray method together with studying as well as comparing the structural, surface morphology, optical and electrical characterizations.

## 2 Experimental

Analytical grade precursor copper chloride ( $\text{CuCl}_2$ , 0.1 M),  $\text{AlCl}_3$ ,  $\text{GaCl}_3$ , and  $\text{InCl}_3$  were used in this work. Distilled water was used as a solvent throughout the experimental procedures. The process of spray deposition was optimized for the best deposition of thin films such as the substrate temperature being fixed at  $450 \text{ }^\circ\text{C}$  and air pressure of  $1.5 \text{ kg/cm}^2$ . The distance from the substrate to the nozzle was kept constant at 5 cm. Figure 1 illustrates the schematic for the synthesis of the CuO and X-doped CuO thin films where the X is Al(1%), Ga(1%), and In(1%). The Al, Ga and In doping thin films are named CuO:Al(1%), CuO:Ga(1%), and CuO:In(1%), respectively.

The coated thin films were subjected to characterization using advanced techniques. To understand the thin films' purity, phase, and crystallization, an X-ray diffractometer (Bruker -D2 with Cu- $K\alpha$  source,

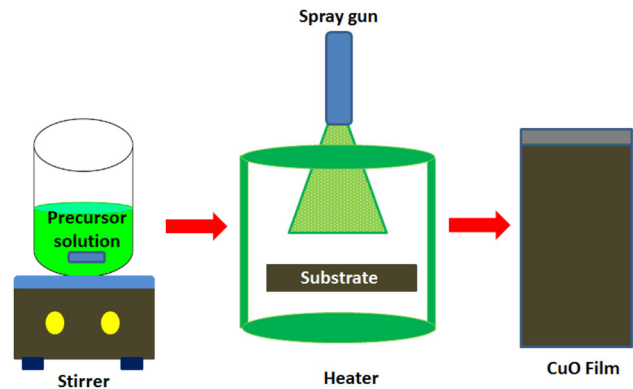


**Fig. 1** Schematic diagram of CuO thin film coating process

$\lambda = 1.5406 \text{ \AA}$ ) was used. The surface morphology of the coated films on glass substrate was studied by field emission-scanning electron microscope (Carl Zeiss Ultra 55). Perkin Elmer LS-55 fluorescence spectrophotometer is used for optical studies such as photoluminescence. UV-spectrophotometer (Perkin Elmer 4 Lambda 35) was used to collect the absorption data in the wavelength range of 300–900 nm. A Keithley source meter (Model 2450) was used to measure the photocurrent characteristics of the prepared thin films. A stylus profilometer (Mitutoyo SJ-301) was used for film thickness measurements of the prepared films. The measured film thickness values are 400, 450, 430 and 410 nm for CuO, CuO:Al (1%), CuO:Ga (1%), and CuO:In (1%) thin films, respectively.

## 3 Results and discussion

### 3.1 Structural studies

Figure 2 shows the XRD patterns of CuO, CuO:Al (1%), CuO:Ga (1%), and CuO:In (1%) thin films, which reveals a typical monoclinic CuO structure with a space group of  $C_{2/c}$ . The diffraction peaks at (110), (002), (111), (020), (202), and (113) are indexed to the pure CuO phase (as per JCPDS file No: 89-5899). The observed high-intensity diffraction peaks suggest the crystallinity nature of CuO of the thin films. Further, the doping does not change the XRD pattern of the host CuO thin film stating that there is no change of structure on doping of Al (1%), Ga (1%), and In (1%). It is seen that doping of Al to the CuO thin films has increased the intensity of the prominent peaks whereas Ga and In doping in CuO

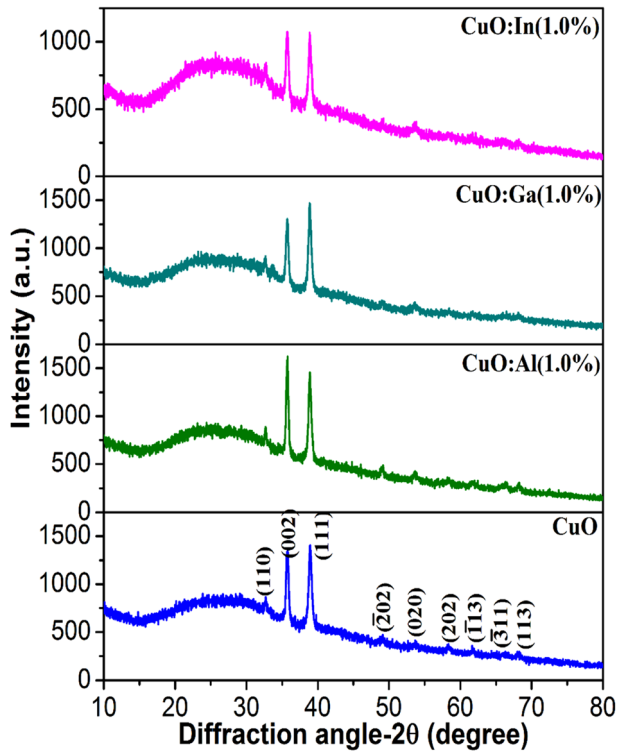


**Fig. 2** XRD patterns of (a) CuO, (b) CuO:Al (1%), (c) CuO:Ga (1%), and (d) CuO: In (1%) thin films prepared by spray method

thin films resulted in the reduction of intensity. The increment in the peak intensity of the (002) plane compared to other thin films, might be due to the lesser ionic radius of Al<sup>3+</sup> (0.54 Å) than Ga<sup>3+</sup> (0.62 Å) and In<sup>3+</sup> (0.80 Å); while the host Cu<sup>2+</sup> ionic radius is (0.74 Å). Therefore, the solubility limit of Al ions is higher than other dopants and hence effortlessly substitutes in the Cu sites. However, the dopant of In<sup>3+</sup> ions may segregate around the grain boundaries of CuO due to its higher atomic size than host Cu<sup>2+</sup> ions, resulting there is a reduction in peak intensity occurs. With reference to XRD patterns, the lattice parameter, the crystallite size (*D*), and strain (*ε*) values of all the films are calculated by given Scherer and Williamson–Hall equations and summarized in Table 1.

$$D = \frac{0.9\lambda}{\beta \cos\theta} \tag{1}$$

$$\epsilon = \frac{\beta \cot\theta}{4}, \tag{2}$$

Where *λ*—X-ray wavelength, *θ*—Bragg angle, *β*—full width half maximum (FWHM). The crystallite size of CuO, CuO:Al (1%), CuO:Ga (1%), and CuO:In (1%) thin films was found to be 33, 41, 36, and 34 nm,

respectively. The strain value decreases by adding impurities with CuO. The maximum crystallite size and minimum strain values obtained by Al doping with CuO are expected to be potential for photo-sensing applications. Rietveld refinement was performed using DIFFRAC.TOPAS v.6.0 (Bruker AXS, Karlsruhe, Germany) software for analyzing the structural parameters which are shown in Supplementary Figure S1. The value of lattice parameters (*a*, *b*, *c*) well matches with early reports for pure CuO thin films [24]. There is a minor variation of lattice parameters after doping of Al, Ga, and In, that is reflected in nearly a constant cell volume. Thus, the XRD results confirmed the incorporation of Al, Ga, and In into the CuO lattice and the effect of doping on the structural pattern of host thin films. The change in a lattice structure and strain by doping metals into CuO have been earlier reported by various research groups [10, 39–41] and matched with the present work.

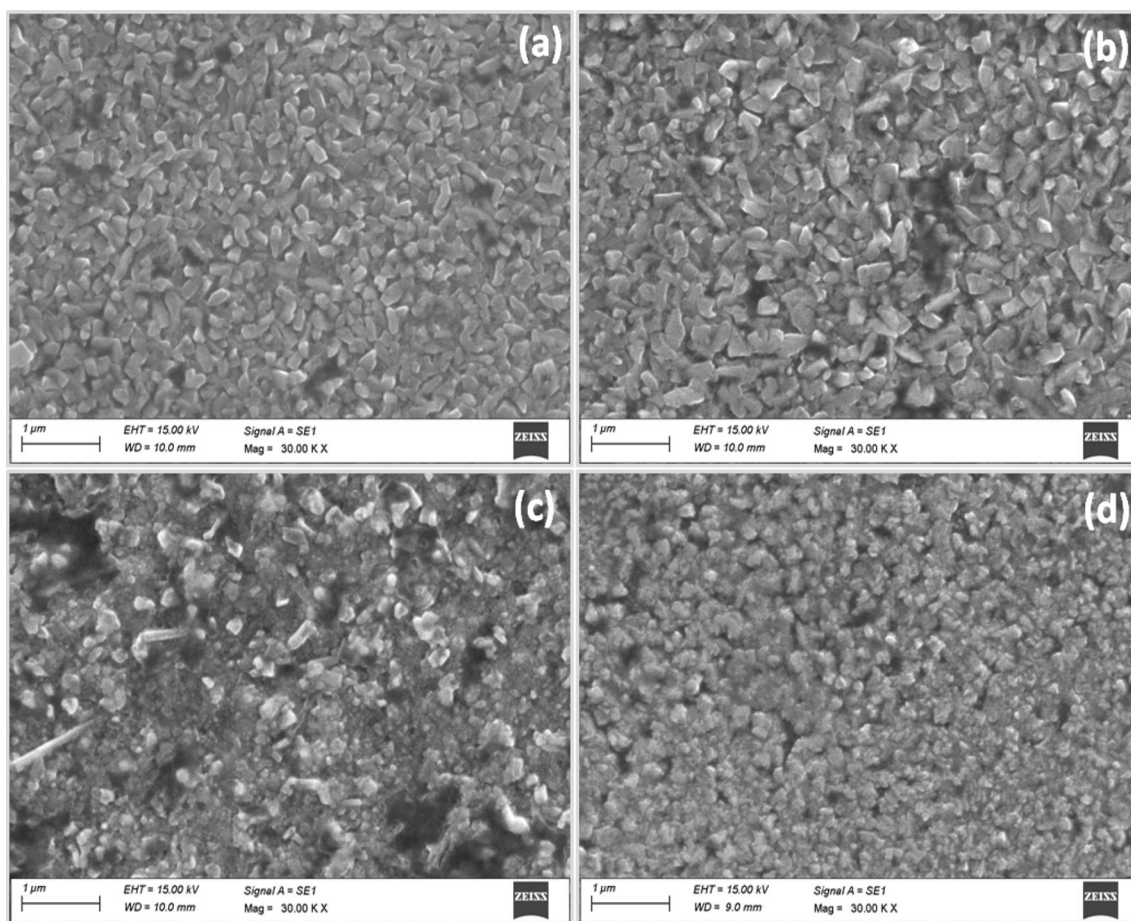
### 3.2 Morphology studies

Figure 3 represents the FESEM micrographs of the CuO, CuO:Al (1%), CuO:Ga (1%), and CuO:In (1%) thin films. The thin film morphology plays a vivacious role in determining the optoelectronic properties. A flaky morphology is seen in Fig. 3a, b whereas agglomerated morphology is seen in Fig. 3c, d. It is clearly seen that the CuO (Fig. 3a) and Al-doped of CuO thin films (Fig. 3b) are nearly similar which substantiates the XRD pattern of CuO and Al-doped CuO thin films. The doping of Ga and In into CuO thin films seems to be slightly changed from the host CuO morphology, which corroborates the XRD analysis. A clear agglomeration of particles is seen for CuO:Ga(1%) and CuO:In (1%) thin films evident a little change in the growth of CuO thin films, as seen in XRD of thin films. Fascinatingly, the Al doping with CuO thin films has formed homogeneous nanoparticles grown on the substrate. The flaky ribbon-type nanoparticles have been widely distributed over the surface of the substrate forming a uniform thin film. Such surfaces that resulted after doping of CuO thin film are expected to show remarkable optoelectronic properties. To understand the elemental composition and amount of doping, the EDX analysis was performed on thin films. The EDX spectra of the fabricated thin films are shown in Fig. 4. The insets of Fig. 4 show the elemental



**Table 1** Crystallite size, strain, lattice constant, and cell volume of the CuO, CuO:Al (1%), CuO:Ga (1%), and CuO:In (1%) thin films

Samples	Crystallite size(nm)	Strain $\times 10^{-3}$	Lattice constant			Cell volume $V(\text{\AA}^3)$
			$a(\text{\AA})$	$b(\text{\AA})$	$c(\text{\AA})$	
CuO	33	3.18	4.674 (4)	3.426 (3)	5.117 (4)	80.87 (11)
CuO:Al(1.0%)	41	2.54	4.663 (6)	3.424 (4)	5.118 (7)	80.66 (18)
CuO:Ga(1.0%)	36	2.89	4.668 (5)	3.423 (4)	5.119 (6)	80.76 (15)
CuO:In(1.0%)	34	3.07	4.686 (7)	3.424 (5)	5.073 (7)	80.30 (2)



**Fig. 3** FESEM images of **a** CuO, **b** CuO:Al (1%), **c** CuO:Ga (1%), and **d** CuO:In (1%) thin films

composition of the fabricated thin films. The Al, Ga, and In doping contents are about 0.94%, 0.87%, and 0.91%, respectively.

### 3.3 Optical studies

The fabricated thin films were subjected to optical properties investigations through optical absorbance in the wavelength range of 300–900 nm which is shown in Fig. 5a. The UV–Vis spectra show a broad

peak in the range of 350–380 nm for all the thin films. Usually, an intense peak with plateau-type UV-absorption spectrum is seen in well crystalline CuO thin films [42, 43]. There is a slight red shift of the peaks observed for doped CuO thin films. The CuO:Al thin film has shown a high intensity absorbance peak compared to other doped thin films. This indicates that Al doping in the CuO host enhances the optical properties due to the change that occurred in grain size and surface morphology of the thin film which is well correlated with the results observed in XRD and

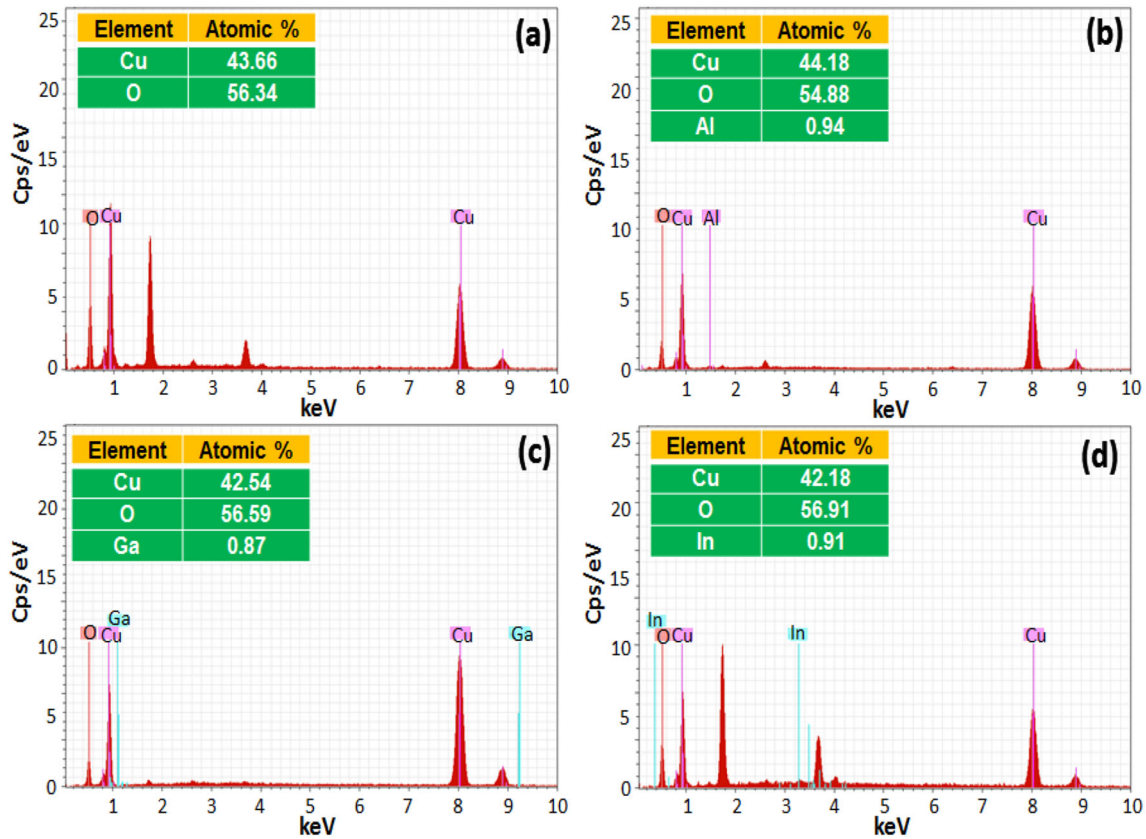


**Fig. 4** EDX spectra of **a** CuO, **b** CuO:Al (1%), **c** CuO:Ga (1%), and **d** CuO:In (1%) thin films (Insets show the corresponding elemental composition)

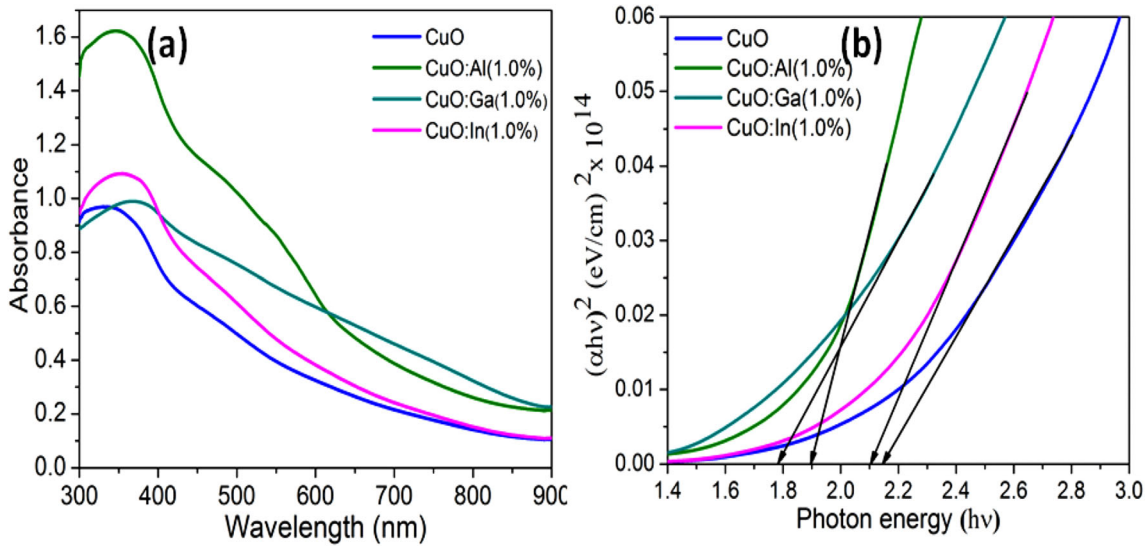


**Fig. 5** **a** Absorption spectra and **b**  $(\alpha h\nu)^2$  vs. photon energy ( $h\nu$ ) curves with linear fits of (a) CuO, (b) CuO:Al (1%), (c) CuO:Ga (1%), and (d) CuO:In (1%) thin films

FESEM studies. It is observed from Fig. 5a that the doping of Al, Ga, and In into the CuO lattice considerably altered the absorbance of pure CuO thin

film, which confirms the improved optical response. The direct band-gap has been calculated by giving Tauc’s relation [22]:

$$\alpha hv = B(hv - E_g)^n, \quad (3)$$

Where  $\alpha$  denotes the absorption coefficient,  $h\nu$  is the incident photon energy,  $B$  is a constant,  $n$  is an index depending upon the nature of the electronic transition responsible for the absorption, and  $E_g$  denotes the bandgap. Figure 5b shows the  $(\alpha hv)^2$  vs. photon energy ( $h\nu$ ) plots for the thin films. The  $E_g$  values of thin films are estimated by extrapolating the linear fit onto the photon energy axis in the high slope region and given in Table 2. The band-gap of pure CuO thin film is found to be 2.14 eV. The  $E_g$  values for CuO:Al (1%), CuO:Ga(1%), and CuO:In (1%) thin films are found to be 1.89, 1.78, and 2.11 eV, respectively. The doping of Al has extraordinarily reduced the band-gap which is due to the decrease in strain value and uniform surface morphology as studied in XRD and FESEM studies. Similarly, doping of trivalent  $Nd^{3+}$  rare-earth to CuO thin films has reduced the bandgap from 2.04 to 1.89 eV [10]. Such doping can affect the optical properties of CuO thin films and be beneficial for light-dependent applications [23, 27].

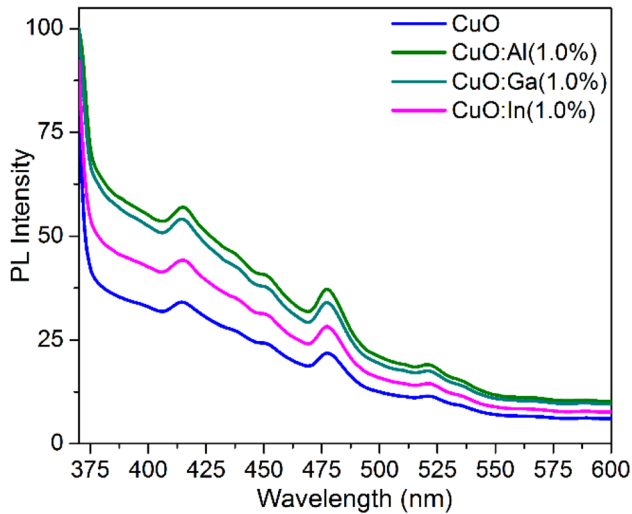
### 3.4 Photoluminescence studies

Figure 6 shows the photoluminescence spectra of as-prepared CuO and doped CuO thin films recorded in the range of 370–600 nm with an excitation wavelength of 350 nm. The doped and undoped thin films exhibited four emission peaks around 410, 450, 475, and 525 nm. The violet emission peak around  $\sim 410$  nm might be because of the recombination of electron-hole pairs due to free-excitons [44]. The blue

emission peak around 450 nm and a broad peak at  $\sim 475$  nm could be due to the electronic transition between the oxygen interstitials and Cu vacancies [45]. A green emission peak around  $\sim 525$  nm might be attributed to the CuO band-band transition, trapped electrons at the defect sites, copper interstitials, oxygen vacancies, and electron transition near the conduction band (CB) [46]. There is an increase in the intensity of the peaks that can be ascribed due to the addition of impurities to the CuO host material. It is worthy to note that, Al-doped CuO exhibits higher intensity peaks than the other doped thin film samples. This is due to the fact that the Al inclusion in the CuO matrix creates Cu vacant sites and oxygen vacant sites. This enhances the optical and in turn, improves the optoelectronic properties of the CuO. This is in accordance with the observations of XRD, FESEM and UV studies. According to Devi et al., the doping of La to the CuO thin film has generated defects in the CuO lattice structure [42]. Muthukrishnan et al. has reported PL intensity variation with a change of concentration of CuO thin films prepared by spray pyrolysis method [18]. The Au-doping to CuO thin films cause a change in the grain boundary and microstrain defects have led to the changes in PL intensity and position of emission peaks [27]. From the PL studies, it is observed that doping of Al improves the morphology as well as defect levels and decrease the bandgap of the CuO film deposited on the substrate which may result in an increment of photoresponse/current of the thin film and matched with the literature [29].

**Table 2** Comparison table showing the photocurrent, dark current, responsivity, external quantum efficiency, detectivity, rise and fall time for CuO, CuO:Al (1%), CuO:Ga (1%), and CuO:In (1%) thin films with other reported works

Samples	$I_{\text{dark}}$ (A)	$I_{\text{photo}}$ (A)	$R(AW^{-1})$	EQE (%)	$D^*$ (Jones)	Rise time (s)	Fall time (s)	References
CuO/Si	3.50 E-11	2.23 E-07	–	–	–	0.85	0.83	[46]
SiO <sub>2</sub> @ CuO/Si	4.78 E-06	1.00 E-04	2.59 E-01	100.7	1.71 E + 12	–	–	[47]
Ni-doped CuO	–	6.00 E-07	26.4 E-00	5176	–	–	–	[32]
CuO-ZnO core shell nanowires	3.43 E-12	$\sim$ E-09	8.74 E-00	26.56	40.5E + 09	$\sim$ 35	$\sim$ 35	[48]
SnO <sub>2</sub> /CuO	$\sim$ E-08	$\sim$ E-05	10.3 E-00	–	–	–	–	[49]
CuO@CuS/Si	–	–	7.98 E-01	309.66	8.19 E + 11	–	–	[50]
CuO	1.35E-06	1.79E-06	8.71E-02	20.0	4.19E + 09	4.6	4.1	
CuO:A l(1.0%)	1.18E-06	2.59E-06	2.82E-01	66.0	1.45E + 10	4.3	4.0	This work
CuO:Ga (1.0%)	1.27E-06	1.73E-06	9.25E-02	22.0	4.59E + 09	4.4	3.9	
CuO:In (1.0%)	1.19E-06	1.78E-06	1.17E-01	27.0	5.99E + 09	4.4	4.0	



**Fig. 6** Photoluminescence spectra of CuO, CuO:Al (1%), CuO:Ga (1%), and CuO:In (1%) thin films

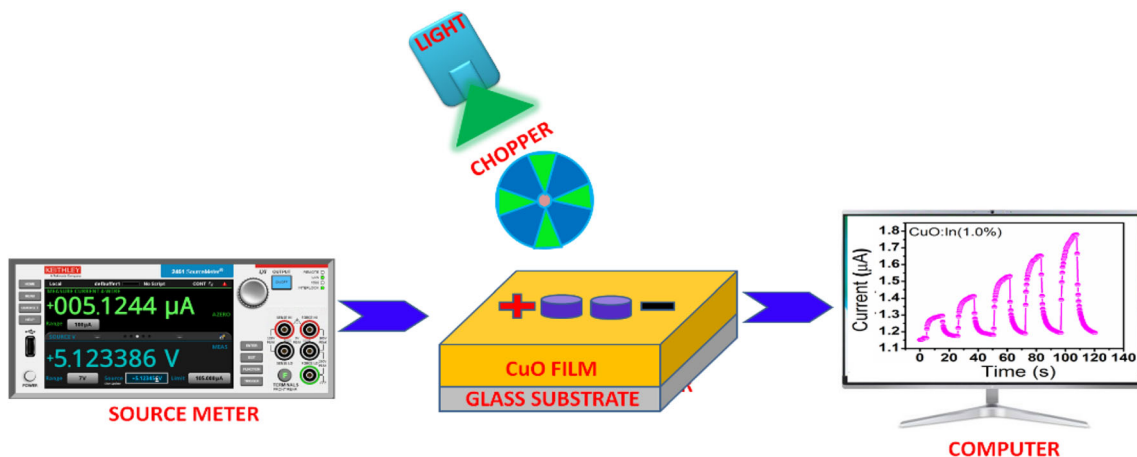
### 3.5 Photo-sensing properties

Figure 7 shows the schematic illustration of photo-sensing studies performed on the fabricated thin films. The  $I$ - $V$  characteristics studied for all the thin films are shown in Fig. 8. The  $I$ - $V$  curves are drawn by varying the bias voltages from + 5 to - 5 V under dark and UV light illumination (365 nm) conditions. The linear trend in  $I$ - $V$  curves is found in the pure CuO and doped CuO thin films. Such a linear trend has been seen in other semiconductor thin films suggesting that the fabricated thin films exhibit ohmic nature. According to Baturay et al., Ni-doped

CuO thin films are reported with low resistivity due to vacancies generated by the dopant element on the host matrix [41]. Similarly, Naveena et al., reported that doped CuO thin films by chemical spray method have displayed high absorption of light which leads to high photocurrent [10]. The  $I$ - $V$  curves of dark current ( $I_{\text{dark}}$ ) and photocurrent ( $I_{\text{photo}}$ ) for the fabricated thin films are recorded in Table 2. The photocurrent is higher than the dark current which indicates that the generation of charge carriers depends on the activation of the light source with respect to the external bias voltage applied. However, the doping of Al, Ga, and In in the CuO host have successfully enhanced both dark and photo-current of the prepared thin films. The photo-current of CuO:Al (1%) is found to be the highest as compared to pure CuO, CuO:Ga (1%), and CuO:In (1%). This can be understood by the previous XRD, FESEM, UV and PL observations such as increment of crystallite and grain size, decrement of the optical bandgap and defects which improves the photosensing ability of the Al-doped CuO thin film compared to the other thin films.

Moreover, the characteristics of the fabricated thin film photodetectors were examined by the photo-sensing parameters viz. responsivity ( $R$ ), detectivity ( $D^*$ ), and external quantum efficiency (EQE). These parameters are calculated by the following formulae (4, 5 and 6) and displayed in Fig. 9.

$$R = \frac{I_p}{P_{in} \times A} \tag{4}$$



**Fig. 7** Schematic illustration of CuO-based thin film photodetector



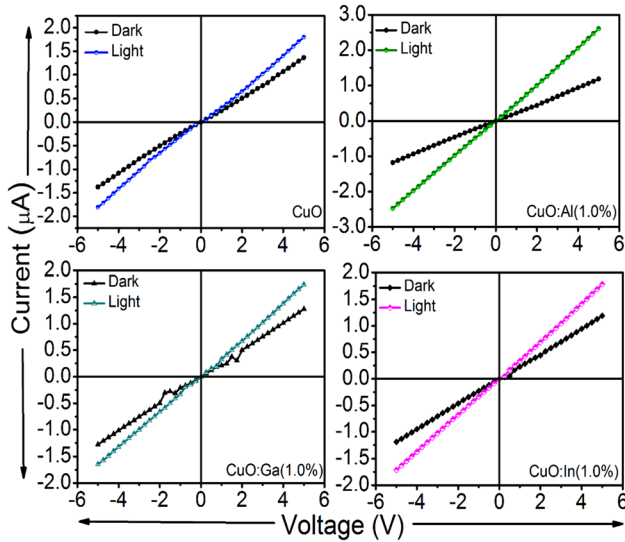


**Fig. 8** Current (*I*)–voltage (*V*) curves of CuO, CuO:Al (1%), CuO:Ga (1%), and (d) CuO:In (1%) photo-detectors measured in dark and presence of light

$$EQE = R \frac{hc}{e\lambda} \tag{5}$$

$$D^* = R \sqrt{\frac{A}{2eI_{dark}}} \tag{6}$$

where  $I_p$ ,  $A$ , and  $P_{in}$  denote the photocurrent, effective area, and power of the light incident over the effective area, respectively. Whereas,  $h$ ,  $c$ , and  $\lambda$  represent Planck’s constant, velocity of light, and wavelength of the incident light, respectively. The symbols  $e$  and  $I_d$  denote the charge of the electron and dark current, respectively. The calculated values

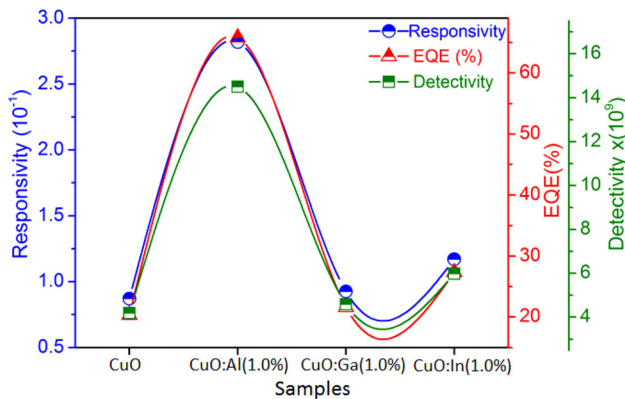


**Fig. 9** Responsivity, external quantum efficiency and detectivity of CuO, CuO:Al (1%), CuO:Ga (1%), and (d) CuO:In (1%) photo-detectors

for  $R$ ,  $D^*$ , and EQE for all the thin films are shown in Fig. 9. The plotted graph infers the values of responsivity of the thin films are found to be  $8.71 \times 10^{-2}$ ,  $2.82 \times 10^{-1}$ ,  $9.25 \times 10^{-2}$ , and  $1.17 \times 10^{-1} \text{ AW}^{-1}$  for CuO, CuO:Al (1%), CuO:Ga (1%), and CuO:In (1%), respectively. Similarly, the EQE values follow the values of 20, 66, 22, and 27% for the above thin films, respectively. The value of  $D^*$  for CuO:Al (1%) is found to be  $1.45 \times 10^{10}$  Jones. Thus, the photodetector parameters elucidate the effect of Al doping on CuO thin films.

The transient photoresponse has been recorded for fabricated CuO-based thin films and shown in Fig. 10. The photoresponse gives the current response of the thin films with respect to the time of ON/OFF condition of light illumination along with the variation of the output power of the light source. The CuO, CuO:Al (1%), CuO:Ga (1%), and CuO:In (1%) photodetectors switched at a 365 nm UV light illumination with the varying power of 1–5  $\text{mW}/\text{cm}^2$ . The systematic rise and fall times with respect to the ON/OFF condition of the light source have been recorded and tabulated in Table 2. The photocurrent response increases with the increasing intensity of the laser light, indicating that more charge carriers were obtained for more intensity of light. The rise time/decay time of the photocurrent for CuO and Al, Ga, In-doped CuO films were found to be 4.6s/4.1s, 4.3s/

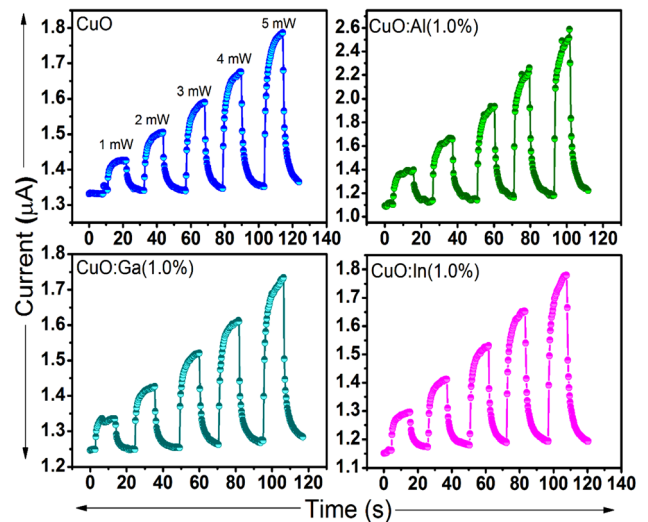


**Fig. 10** Time-dependent photo-response (Current vs. time) of CuO, CuO:Al (1%), CuO:Ga (1%) and CuO:In (1%) photo-detectors switched at a 365 nm UV light illumination with the power of 1–5  $\text{mW}/\text{cm}^2$ . ON and OFF periodically at a fixed bias field of 5 V

4.0s, 4.4s/3.9 and 4.4s/4.0s, respectively. The Al-doped CuO thin film has a minimum value of rise/decay time as compared to other thin films that are due to the improved crystallinity and well-grown thin film with a uniform surface. The mechanism for the observed changes in the photosensitive properties of present thin films as a function of doping material can be explained and is attributed to the number of oxygen molecules available for the adsorption and desorption process at the surface of the films as well as carrier concentration differences caused by the intrinsic nature of dopant elements. Since CuO:Al (1%) exhibits a highly crystalline nature and surface homogeneity from the studies of XRD and FESEM as compared to the other films, which suggests the increment of photosensing behavior. Optical and PL studies showed that the increment of PL intensity and least bandgap enrich the photo-induced charge carriers in Al-doped CuO thin film compared to the other prepared thin films. As a result, CuO:Al (1%) exhibits relatively better photo-sensing properties among all the fabricated thin films. The photodetector thin film is reported with high photocurrent due to high charge carriers [16]. The oxygen vacancies lead to excellent visible-light absorption and electron-hole pair generation/recombination. A similar doping effect is seen in C and Au doped CuO thin film [11, 12]. The Comparison of photocurrent, dark current, responsivity, external quantum efficiency, detectivity, rise and fall time for CuO, CuO:Al (1%), CuO:Ga (1%), and CuO:In (1%) thin films with other reported works was given in Table 2. Thus, the present study reveals the significance of doping elements on the structural, optical and photo-sensing properties of CuO thin films.

### 3.6 Mechanism of CuO thin film photodetector

The photoresponse of the fabricated photodetector could be explained using the mechanism shown in Fig. 11. The explanation of the charge transfer process of the metal oxide-based photodetector was carried out in dark and light conditions at a bias voltage of 5 V. During the dark conditions, oxygen atoms are adsorbed to the surface of CuO creating electron trap sites ( $O_2 + e^- = O_2^-$ ). These trap sites result in the formation of a wider depletion layer in turn reducing the electrical conductivity resulting in the decrease of dark current value. Moreover, when

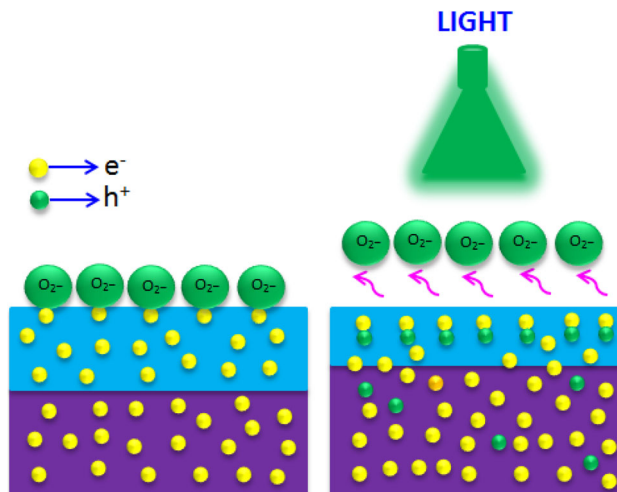


**Fig. 11** Mechanism showing the photoresponse of the fabricated metal oxide-based photodetector

the photodiode was exposed to UV light, the photo-generated carriers (i.e., holes) neutralize the surface oxygen ions ( $h^+ + O_2^- = O_2$ ) making the electrons free from recombination with holes. This phenomenon increases the life time of the electrons and in turn, increases the photocurrent value. When the light is cut off, the oxygen ions are again adsorbed to the CuO surface and the resultant current value decreases.

## 4 Conclusions

The effect of Al, Ga, and In doping in structural, morphological, optical, and photosensing properties of pure CuO thin films fabricated by spray technology. The doped CuO thin films were optimized for photosensing applications. The CuO, CuO:Al (1%), CuO:Ga (1%), and CuO:In (1%) thin films are found to be crystalline and flaky morphology. The optical properties revealed that the CuO:Al(1%) thin film's highest optoelectronic property in comparison to the CuO, CuO:Ga (1%), and CuO:In (1%) thin films. The photosensing parameters responsivity, detectivity, and external quantum efficiency of the Al-doped CuO thin film exhibited higher values among the other samples which were found to be  $2.82 \times 10^{-1} \text{ AW}^{-1}$ ,  $1.45 \times 10^{10} \text{ Jones}$  and 66%, respectively. The doping of Al with CuO thin films has improved optoelectronic properties, which can be utilized for photodetectors. This work opens the scope for the

investigation of other parameters to boost the performances of photodetectors.

## Acknowledgements

The authors from KSU extend their sincere appreciation to the Researchers Supporting Project No (RSP-2022/55), King Saud University, Riyadh, Saudi Arabia for the support.

## Author contribution

TG, SV—Conceptualization, Data curation, Formal analysis, Writing—original draft, HTD—Writing—review and editing. NC—Formal analysis, Writing, RSRI—Data curation, Formal analysis. AMAIE, MU, VRMR—Funding acquisition, Investigation, Methodology, Project administration,

## Data availability

The datasets generated during and/or analysed during the current study are available from the corresponding author on reasonable request.

## Declarations

**Conflict of interest** The authors report no conflicts of interest.

**Supplementary Information:** The online version contains supplementary material available at <http://doi.org/10.1007/s10854-022-08728-2>.

## References

1. L. Shi, F. Wang, B. Li, X. Chen, B. Yao, D. Zhao, D. Shen, J. Mater. Chem. C **2**, 5005 (2014)
2. L. Li, L. Gu, Z. Lou, Z. Fan, G. Shen, ACS Nano **11**, 4067 (2017)
3. D.J. Lee, G.M. Kumar, Y. Kim, W. Yang, D.Y. Kim, T.W. Kang, P. Ilanchezhian, J. Mater. Res. Technol. **18**, 4946 (2022)
4. J. Wang, S. Lee, Sensors **11**, 696 (2011)
5. X. Zhao, G. Wang, H. Lin, Y. Du, X. Luo, Z. Kong, J. Su, J. Li, W. Xiong, Y. Miao, H. Li, G. Guo, H.H. Radamson, Nanomaterials **11**, (2021)
6. I.L.P. Raj, S. Valanarasu, A. Asuntha, R.S. Rimal Isaac, M. Shkir, H. Algarni, S. AlFaify, J. Mater. Sci. Mater. Electron. **33**(5), 11753 (2022)
7. R. Molavi, M.H. Sheikhi, Mater. Sci. Semicond. Process. **106**, 104767 (2020)
8. T.E. Balaji, H.Tanaya Das, T. Maiyalagan, ChemElectroChem **8**, 1723 (2021)
9. B. Yan, Y. Wang, T. Jiang, X. Wu, J. Mater. Sci. Mater. Electron. **27**, 5389 (2016)
10. D. Naveena, T. Logu, R. Dhanabal, K. Sethuraman, A.C. Bose, J. Mater. Sci. Mater. Electron. **30**, 561 (2019)
11. M.M. Koc, J. Mol. Struct. **1208**, 127872 (2020)
12. S. Ruzgar, Y. Caglar, O. Polat, D. Sobola, M. Caglar, Surf. Interfaces **21**, 100750 (2020)
13. Z. Zang, A. Nakamura, J. Temmyo, Mater. Lett. **92**, 188 (2013)
14. C. Ravichandiran, A. Sakthivelu, R. Davidprabu, K. Deva Arun Kumar, S. Valanarasu, A. Kathalingam, V. Ganesh, M. Shkir, S. AlFaify, Thin Solid Films **683**, 82 (2019)
15. I.A. Zgair, A.H. Omran Alkhayatt, A.A. Muhmood, S.K. Hussain, Optik (Stuttg). **191**, 48 (2019)
16. S.K. Shaikh, V.V. Ganbavle, S.I. Inamdar, K.Y. Rajpure, RSC Adv. **6**, 25641 (2016)
17. W.Q. Liang, Y. Li, J.L. Ma, Y. Wang, J.J. Yan, X. Chen, D. Wu, Y.T. Tian, X.J. Li, Z.F. Shi, Nanoscale **12**, 17213 (2020)
18. S. Muthukrishnan, V. Subramaniam, T. Mahalingam, S.J. Helen, P. Sumathi, J. Mater. Sci. Mater. Electron. **28**, 4211 (2017)
19. B. Das, K. Sa, P. Chandra Mahakul, B.V.R.S. Subramanyam, S. Das, I. Alam, J. Raiguru, P. Mahanandia, Superlattices Microstruct. **123**, 234 (2018)
20. H. Bae, A. Charnas, X. Sun, J. Noh, M. Si, W. Chung, G. Qiu, X. Lyu, S. Alghamdi, H. Wang, D. Zemlyanov, P.D. Ye, ACS Omega **4**, 20756 (2019)
21. J. Hun Yu, W.J. Lee, D.H. Cho, W.J. Kim, S. Jun, Kang, Y.D. Chung, Appl. Surf. Sci. **590**, 153062 (2022)
22. P. Gu, X. Zhu, D. Yang, RSC Adv. **9**, 8039 (2019)
23. M. Shkir, M. Arif, V. Ganesh, A. Singh, H. Algarni, I.S. Yahia, S. AlFaify, Appl. Phys. A Mater. Sci. Process **126**, 1 (2020)
24. H.T. Das, S. Vinoth, M. Thirumoorthi, T. Alshahrani, H.H. Hegazy, H.H. Somaily, M. Shkir, S. AlFaify, J. Inorg. Organomet. Polym. Mater. **31**, 2606 (2021)
25. A. Badawi, S.S. Alharthi, M.G. Althobaiti, A.N. Alharbi, H. Assaedi, H.I. Alkhamash, N. Al-Hosiny, Appl. Phys. A Mater. Sci. Process. **127**, 1 (2021)
26. S.S.K. Jacob, I. Kulandaisamy, S. Valanarasu, A.M.S. Arulanatham, V. Ganesh, M. Shkir, I.S. Yahia, Mater. Res. Express **6**, 115055 (2019)

27. R.A. Ismail, R.S. Abdul-Hamed, *Mater. Res. Express* **4**, 125020 (2017)
28. C. Ravichandiran, A. Sakthivelu, R. Davidprabu, K. Deva Arun Kumar, S. Valanarasu, A. Kathalingam, V. Ganesh, M. Shkir, H. Algarni, S. AlFaify, *J. Sol-Gel Sci. Technol.* **578** (2019)
29. C.R.A. Sakthivelu, K.D. Arun, K.R. Davidprabu, S.V.A. Kathalingam, *J. Mater. Sci. Mater. Electron.* **30**, 2530 (2019)
30. M.R. Islam, J.E. Obaid, M. Saiduzzaman, S.S. Nishat, T. Debnath, A. Kabir, *J. Phys. Chem. Solids* **147**, 109646 (2020)
31. Y. Du, X. Meng, X. Gao, *Thin Solid Films* **684**, 53 (2019)
32. W. Yin, J. Yang, K. Zhao, A. Cui, J. Zhou, W. Tian, W. Li, Z. Hu, J. Chu, *ACS Appl. Mater. Interfaces* **12**, 11797 (2020)
33. J. Mathew, S. Devasia, S. Shaji, E.I. Anila, *Optik (Stuttg)* **241**, 166878 (2021)
34. V. Doni Pon, K.S. Joseph Wilson, K. Hariprasad, V. Ganesh, H. Elhosiny, H. Ali, Algarni, I.S. Yahia, *Superlattices Microstruct.* **151**, 7 (2021)
35. L. Fan, Z. Cheng, J. Du, P. Delir Kheirollahi Nezhad, *Monatshefte Für Chemie—Chem. Mon.* **153**(4), 321 (2022)
36. T. Weng, M. Yan, X. Yu, Q. Qiao, Y. Zhou, Z. Li, J. Wei, X. Yu, *Opt. Mater. (Amst)* **121**, 111516 (2021)
37. J.H. Bae, J.H. Lee, S.P. Park, T.S. Jung, H.J. Kim, D. Kim, S.W. Lee, K.S. Park, S. Yoon, I. Kang, H.J. Kim, *ACS Appl. Mater. Interfaces* **12**, 38350 (2020)
38. S. Baturay, A. Tombak, D. Batibay, Y.S. Ocak, *Appl. Surf. Sci.* **477**, 91 (2019)
39. W.Z. Tawfik, Z.S. Khalifa, M.S. Abdel-wahab, A.H. Hammad, *J. Mater. Sci. Mater. Electron.* **30**, 1275 (2019)
40. S. Baturay, A. Tombak, D. Kaya, Y.S. Ocak, M. Tokus, M. Aydemir, T. Kilicoglu, *J. Sol-Gel Sci. Technol.* **78**, 422 (2016)
41. L.V. Devi, T. Selvalakshmi, S. Sellaiyan, A. Uedono, K. Sivaji, S. Sankar, *J. Alloys Compd.* **709**, 496 (2017)
42. A. Tombak, M. Benhaliliba, Y.S. Ocak, T. Kiliçoglu, *Results Phys.* **5**, 314 (2015)
43. P. Chand, A. Gaur, A. Kumar, U. Kumar, Gaur, *Appl. Surf. Sci.* **307**, 280 (2014)
44. A.R. Ansari, A.H. Hammad, M.S. Abdel-wahab, M. Shariq, M. Imran, *Opt. Quantum Electron* **52**, 1 (2020)
45. C.R. Gobbiner, G.R. Dillip, S.W. Joo, D. Kekuda, *Ceram. Int.* **44**, 16984 (2018)
46. J. Sultana, S. Paul, A. Karmakar, G.K. Dalapati, S. Chattopadhyay, *J. Mater. Sci. Mater. Electron.* **29**, 12878 (2018)
47. S. Gunasekaran, D. Thangaraju, R. Marnadu, J. Chandrasekaran, T. Alshahrani, M. Shkir, A. Durairajan, M.P.F. Graça, M. Elango, *Surf. Interfaces* **20**, 100622 (2020)
48. A. Costas, C. Florica, N. Preda, A. Kuncser, I. Enculescu, *Sci. Rep.* **10**, 1 (2020)
49. T. Xie, M.R. Hasan, B. Qiu, E.S. Arinze, N.V. Nguyen, A. Motayed, S.M. Thon, R. Debnath, *Appl. Phys. Lett.* **107**, 241108 (2015)
50. S. Gunasekaran, D. Thangaraju, R. Marnadu, J. Chandrasekaran, M. Shkir, A. Durairajan, M.A. Valente, T. Alshaharanig, M. Elango, *Sens. Actuators Phys.* **317**, 112373 (2021)

**Publisher's Note** Springer Nature remains neutral with regard to jurisdictional claims in published maps and institutional affiliations.